J. Fluid Mech. (2011), *vol.* 667, *pp.* 520–543.
doi:10.1017/S0022112010004507

Planar channel flow in Braginskii magnetohydrodynamics

PAUL J. DELLAR†

OCIAM, Mathematical Institute, 24–29 St Giles', Oxford OX1 3LB, UK

(Received 25 February 2010, revised 3 August 2010; accepted 24 August 2010)

Braginskii magnetohydrodynamics (MHD) is a single-fluid description of large-scale motions in strongly magnetised plasmas. The ion Larmor radius in these plasmas is much shorter than the mean free path between collisions, so momentum transport across magnetic field lines is strongly suppressed. The relation between the strain rate and the viscous stress becomes highly anisotropic, with the viscous stress being predominantly aligned parallel to the magnetic field. We present an analytical study of the steady planar flow across an imposed uniform magnetic field driven by a uniform pressure gradient along a straight channel, the configuration known as Hartmann flow, in Braginskii MHD. The global momentum balance cannot be satisfied by just the parallel viscous stress, so we include the viscous stress perpendicular to magnetic field lines as well. The ratio of perpendicular to parallel viscosities is the key small parameter in our analysis. When another parameter, the Hartmann number, is large the flow is uniform across most of the channel, with boundary layers on either wall that are modifications of the Hartmann layers in standard isotropic MHD. However, the Hartmann layer solution predicts an infinite current and infinite shear at the wall, consistent with a local series solution of the underlying differential equation that is valid for all Hartmann numbers. These singularities are resolved by inner boundary layers whose width scales as the three-quarters power of the viscosity ratio, while the maximum velocity scales as the inverse one-quarter power of the viscosity ratio. The inner wall layers fit between the Hartmann layers, if present, and the walls. The solution thus does not approach a limit as the viscosity ratio tends to zero. Essential features of the solution, such as the maximum current and maximum velocity, are determined by the size of the viscosity ratio, which is the regularising small parameter.

Key words: boundary layers, high-Hartmann-number flows, plasmas

1. Introduction

Magnetohydrodynamics (MHD) is concerned with fluid descriptions of media containing two or more different types of charged particles, such as electrolytes, liquid metals and plasmas. The conventional MHD equations modify the Navier–Stokes momentum equation only through the addition of the Lorentz force. The standard Navier–Stokes form of the viscous stress is left unchanged. However, the phenomenological derivation of the Navier–Stokes equations assumes a linear and isotropic relation between stress and strain rate. This assumption of isotropy breaks down when a magnetic field is present to define a preferred direction. Similarly, the

† Email address for correspondence: dellar@maths.ox.ac.uk

derivation of the Navier–Stokes equations from the Boltzmann equation of kinetic theory is valid only for uncharged particles (Chapman & Cowling 1970; Cercignani 1988). Braginskii MHD extends the conventional MHD equations to account for the anisotropic relations that define the viscous stress and conduction current in a strongly magnetised plasma, one in which the ion Larmor radius is much smaller than the mean free path, and the ion gyrofrequency is much larger than the collision frequency.

A kinetic description of a plasma requires two kinetic equations, one each for the ion and electron distribution functions. Boltzmann's binary collision operator is replaced by the Fokker–Planck collision operator that describes the many glancing collisions mediated by Coulomb interactions between charged particles. Both kinetic equations are further coupled to the electromagnetic field by Lorentz force terms. From this starting point, Braginskii (1965) calculated the viscous stress and conduction current due to large-scale motions in a strongly magnetised, or weakly collisional, plasma. Large-scale motions are those motions whose spatial scale is large, and temporal scale is slow, compared with collisions between ions or electrons in the plasma. Due to their widely separated masses, collisions are much less effective at transferring energy from ions to electrons, or vice versa, than they are at transferring energy between pairs of ions or pairs of electrons. It is thus common to consider regimes in which the ions and electrons may each be treated separately as a fluid, but the coupling between ions and electrons is left explicit. This is often called a 'two-fluid' description. Braginskii's (1965) work improved on that of Chapman & Cowling (1970) by exploiting the small ratio of electron to ion masses, $m_e/m_i \ll 1$, as well as a small mean free path.

Braginskii (1965) found that the relations between stress and strain, and between current and electric field, are indeed anisotropic, with a preferred direction set by the magnetic field. The largest contribution to the viscous stress in the ion fluids is

$$\boldsymbol{\sigma}_0 = 3\eta_0\big(\hat{\boldsymbol{b}}\hat{\boldsymbol{b}} - \tfrac{1}{3}\boldsymbol{I}\big)\,\big(\hat{\boldsymbol{b}}\hat{\boldsymbol{b}} - \tfrac{1}{3}\boldsymbol{I}\big) : \boldsymbol{\nabla u}, \tag{1.1}$$

where η_0 is the parallel viscosity, $\boldsymbol{I}$ is the 3×3 identity matrix, $\hat{\boldsymbol{b}} = \boldsymbol{B}/|\boldsymbol{B}|$ is a unit vector parallel to the magnetic field, and $\boldsymbol{\nabla u}$ is the ion velocity gradient. The colon : denotes a double contraction between two tensors. The contribution in (1.1) is typically much larger than the further contributions to the viscous stress that involve the perpendicular viscosities, and the 'drift' or 'gyro' viscosities, as described in § 2 below. The full relation between stress and strain is much more complicated than as given in (1.1). Stress and strain are both second-rank tensors, so the general linear relation between them requires a fourth-rank tensor, with five independent coefficients, i.e. η_0 to η_4 as defined in § 2 below. The anisotropy arises because a charged particle is constrained to lie close to a magnetic field line. The parallel viscosity η_0 takes the value that it would in an unmagnetised plasma, based on the mean free path between collisions, while the perpendicular viscosity takes a much smaller value based on the ion Larmor radius as an effective mean free path.

For sufficiently large-scale and low-frequency motions, Braginskii's (1965) coupled equations for separate electron and ion fluids may be reduced to a set of single-fluid equations that have been named 'Braginskii magnetohydrodynamics' (see e.g. Schekochihin *et al.* 2005). These equations are described in Lifshitz & Pitaevskii (1981, §§ 58 and 59). They coincide with those of standard resistive magnetohydrodynamics, except the constitutive relations for the viscous stress, heat flux and electric field become anisotropic. The Braginskii MHD equations have recently attracted attention as a model for the very large scale motions of the plasma in and around clusters of galaxies (Schekochihin *et al.* 2005; Lyutikov 2008; Dong & Stone 2009) for galactic

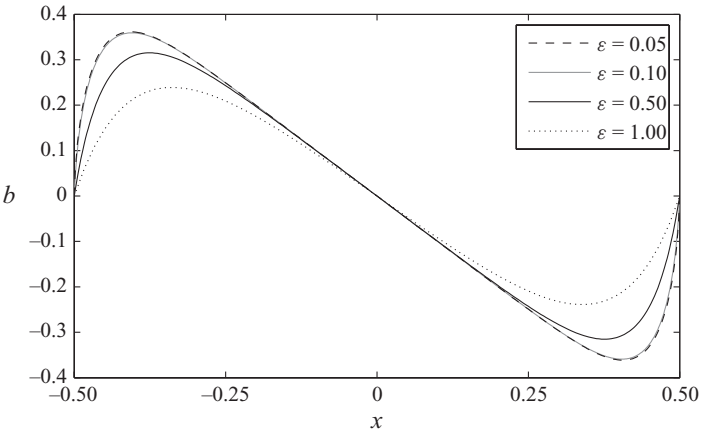

FIGURE 1. Magnetic field $b(x)$ for channel flow with $f = 1$ and $Ha = 10$, in the dimensionless units of §4. The magnetic field appears to have approached a limiting profile for the two different values $\epsilon = 0.1$ and $\epsilon = 0.05$.

disks (Balbus 2004; Islam & Balbus 2005; Sharma *et al.* 2007) and for the solar corona (Hollweg 1986; Craig & Litvinenko 2009). Some experimental evidence for Braginskii's viscosity values has recently been reported by Dorf *et al.* (2007) using the reconnection scaling experiment (Furno *et al.* 2003).

In this paper, we investigate the unidirectional flow of fluid across an imposed magnetic field using the Braginskii MHD equations. This problem, known as Hartmann flow in standard MHD, is the MHD analogue of Poiseuille flow. It is one of the few MHD flows that is analytically tractable (e.g. Landau & Lifshitz 1960; Hunt & Shercliff 1971) because the idealised geometry leads to linear equations without a need to invoke small perturbations. However, the problem as currently posed for Braginskii MHD has no solution, because the viscous stress $\boldsymbol{\sigma}_0$ vanishes on the walls of the channel. We, therefore, regularise the relation (1.1) by including Braginskii's (1965) expressions for the viscous stress in directions perpendicular to the magnetic field. Some regularisation is also needed to suppress the mirror and firehose instabilities in the time-dependent form of Braginskii MHD (Schekochihin *et al.* 2005), although these instabilities do not arise in our study of steady unidirectional flow.

In a recent numerical study of Hartmann flow in Braginskii MHD with a small *ad hoc* regularisation, Lyutikov (2008) asserted that the magnetic and velocity fields approach limits that are independent of the regularisation. Figures 1 and 2 show some numerical solutions for different ratios ϵ of the perpendicular to parallel viscosities. The magnetic field profiles shown in figure 1 for $\epsilon = 0.1$ and $\epsilon = 0.05$ are nearly identical, so it appears plausible that the magnetic field profile is tending towards some limit as $\epsilon \to 0$, However, the corresponding velocity profiles shown in figure 2 are substantially different. The maximum velocity increases substantially as ϵ is reduced from 0.1 to 0.05, although the figure suggests that the *relative* velocities away from the walls may be approaching a limiting profile as $\epsilon \to 0$. The asymptotic analysis presented below shows that the magnetic field and the velocity relative to the centreline do tend to limiting profiles over most of the domain. However, large shears and currents develop in narrow boundary layers on either wall, so the solution as a whole does not approach a limit as the regularising coefficient ϵ tends to zero.

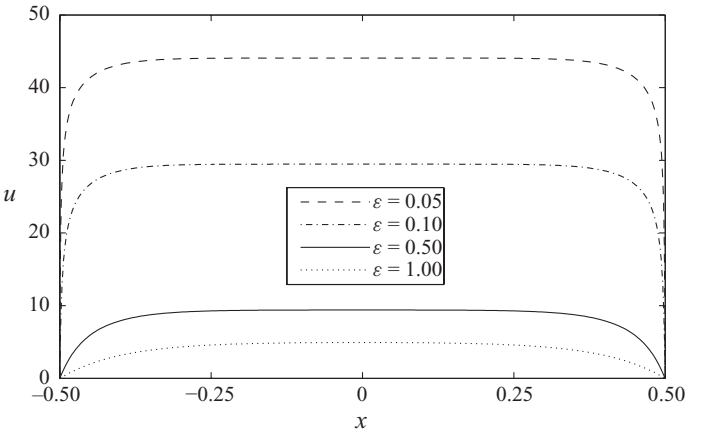

FIGURE 2. Velocity $u(x)$ for channel flow with $f = 1$ and $Ha = 10$, in the dimensionless units of §4. The maximum velocity continues to increase with decreasing ϵ.

2. Braginskii magnetohydrodynamics

Starting from a pair of kinetic equations for the ion and electron distribution functions, Braginskii (1965) derived hydrodynamic equations for separate ion and electron fluids by using the same Chapmann–Enskog expansion that leads from the Boltzmann equation to the Navier–Stokes equations (Chapman & Cowling 1970; Cercignani 1988). Equivalent equations were later obtained by Balescu (1988) using Grad's (1949, 1958) method of moments. Like the Navier–Stokes equations, these equations include the first dissipative corrections from finite mean free path effects. They are valid on time scales much longer than the ion–ion and electron–electron collision times τ_i and τ_e respectively, and on spatial scales much larger than the mean free paths. As mentioned above, collisions between pairs of ions or pairs of electrons exchange momentum and energy much more readily than collisions between ions and electrons. A two-fluid description with separate ion and electron fluids is thus more generally applicable than a single fluid description. In the following, we use the Gaussian electromagnetic units that are commonly employed for Braginskii MHD.

Taking moments of the kinetic equation for ions gives conservation equations for mass, momentum and energy in the ion fluid,

$$\partial_t \boldsymbol{u}_i + \nabla\cdot(n_i\boldsymbol{u}_i) = 0, \tag{2.1a}$$

$$m_i n_i \frac{\mathrm{D}_i \boldsymbol{u}_i}{\mathrm{D}t} = -\nabla(n_i T_i) - \nabla\cdot\boldsymbol{\sigma}_i + e n_i\left(\boldsymbol{E} + \frac{\boldsymbol{u}_i\times\boldsymbol{B}}{c}\right) - \boldsymbol{R}, \tag{2.1b}$$

$$\frac{3}{2} n_i \frac{\mathrm{D}_i T_i}{\mathrm{D}t} + n_i T_i \nabla\cdot\boldsymbol{u}_i = -\nabla\cdot\boldsymbol{q}_i - \boldsymbol{\sigma}_i : \nabla\boldsymbol{u}_i + Q_i, \tag{2.1c}$$

where $\mathrm{D}_i/\mathrm{D}t = \partial_t + \boldsymbol{u}_i\cdot\nabla$ is the material time derivative moving with the ion fluid velocity $\boldsymbol{u}_i$. The other quantities are the ion mass m_i, number density n_i, and temperature T_i, and similarly for the electrons. The elementary charge is e. The equations for the electron fluid are similar, except the Lorentz force and the ion–electron collision term $\boldsymbol{R}$ have the opposite signs. These conservation equations must be supplemented by constitutive relations for the collision term $\boldsymbol{R}$, and the viscous stresses $\boldsymbol{\sigma}_i$ and $\boldsymbol{\sigma}_e$, heat fluxes $\boldsymbol{q}_i$ and $\boldsymbol{q}_e$, and Ohmic heat sources Q_i and Q_e in each

fluid. For example, Braginskii (1965) calculated the ion–electron collision term to be

$$\boldsymbol{R} = -0.71 n_e \nabla_\parallel T_e + n_e e \left(\frac{\boldsymbol{J}_\parallel}{\sigma_\parallel} + \frac{\boldsymbol{J}_\perp}{\sigma_\perp} \right), \tag{2.2}$$

where $\nabla_\parallel T_e$ is the gradient of the electron temperature parallel to the magnetic field. The current $\boldsymbol{J}$ has been decomposed into components $\boldsymbol{J}_\parallel = \hat{\boldsymbol{b}}\hat{\boldsymbol{b}} \cdot \boldsymbol{J}$ and $\boldsymbol{J}_\perp = \boldsymbol{J} - \boldsymbol{J}_\parallel$ parallel and perpendicular to the magnetic field lines. The parallel and perpendicular conductivities are

$$\sigma_\parallel = 1.96\,\sigma_\perp, \quad \sigma_\perp = \frac{e^2 n_e \tau_e}{m_e}, \quad \tau_e = \frac{3}{4\sqrt{2\pi}} \frac{\sqrt{m_e}\, T_e^{3/2}}{n_e\, e^4\, \ln \Lambda}, \tag{2.3}$$

where $\ln \Lambda$ is the Coulomb logarithm (Spitzer 1962). Finally, the two sets of fluid equations are coupled to Maxwell's equations for the electromagnetic field,

$$\partial_t \boldsymbol{B} + c \nabla \times \boldsymbol{E} = 0, \quad \nabla \cdot \boldsymbol{B} = 0, \quad \nabla \times \boldsymbol{B} = \frac{4\pi}{c} \boldsymbol{J}. \tag{2.4}$$

We have assumed non-relativistic motion to omit Maxwell's displacement current, following the standard MHD approximation.

2.1. *The viscous stress*

Braginskii's (1965) expression for the viscous stress may be written as

$$\boldsymbol{\sigma}_i = \eta_0 \boldsymbol{W}^{(0)} + \eta_1 \boldsymbol{W}^{(1)} + \eta_2 \boldsymbol{W}^{(2)} + \eta_3 \boldsymbol{W}^{(3)} + \eta_4 \boldsymbol{W}^{(4)}, \tag{2.5}$$

where η_0 to η_4 are the five viscosities given below. The five separate contributions to the viscous stress may be written as (Hogan 1984)

$$\boldsymbol{W}^{(0)} = \tfrac{3}{2} \left(\hat{\boldsymbol{b}}\hat{\boldsymbol{b}} - \tfrac{1}{3} \boldsymbol{I} \right) \hat{\boldsymbol{b}} \cdot \boldsymbol{W} \cdot \hat{\boldsymbol{b}}, \tag{2.6a}$$

$$\boldsymbol{W}^{(1)} = (\boldsymbol{I} - \hat{\boldsymbol{b}}\hat{\boldsymbol{b}}) \cdot \boldsymbol{W} \cdot (\boldsymbol{I} - \hat{\boldsymbol{b}}\hat{\boldsymbol{b}}) + \tfrac{1}{2} (\boldsymbol{I} - \hat{\boldsymbol{b}}\hat{\boldsymbol{b}}) \hat{\boldsymbol{b}} \cdot \boldsymbol{W} \cdot \hat{\boldsymbol{b}}, \tag{2.6b}$$

$$\boldsymbol{W}^{(2)} = (\boldsymbol{I} - \hat{\boldsymbol{b}}\hat{\boldsymbol{b}}) \cdot \boldsymbol{W} \cdot \hat{\boldsymbol{b}}\hat{\boldsymbol{b}} + \hat{\boldsymbol{b}}\hat{\boldsymbol{b}} \cdot \boldsymbol{W} \cdot (\boldsymbol{I} - \hat{\boldsymbol{b}}\hat{\boldsymbol{b}}), \tag{2.6c}$$

$$\boldsymbol{W}^{(3)} = \tfrac{1}{2} \boldsymbol{B}^\perp \cdot \boldsymbol{W} \cdot (\boldsymbol{I} - \hat{\boldsymbol{b}}\hat{\boldsymbol{b}}) - \tfrac{1}{2} (\boldsymbol{I} - \hat{\boldsymbol{b}}\hat{\boldsymbol{b}}) \cdot \boldsymbol{W} \cdot \boldsymbol{B}^\perp, \tag{2.6d}$$

$$\boldsymbol{W}^{(4)} = (\boldsymbol{B}^\perp \cdot \boldsymbol{W} \cdot \hat{\boldsymbol{b}})\, \hat{\boldsymbol{b}} - \hat{\boldsymbol{b}}\, (\boldsymbol{B}^\perp \cdot \boldsymbol{W} \cdot \hat{\boldsymbol{b}}), \tag{2.6e}$$

where the strain rate $\boldsymbol{W}$ is the symmetric, traceless tensor formed from the ion velocity gradient by

$$\boldsymbol{W} = \nabla \boldsymbol{u}_i + (\nabla \boldsymbol{u}_i)^\mathsf{T} - \tfrac{2}{3} \boldsymbol{I} \nabla \cdot \boldsymbol{u}_i. \tag{2.7}$$

The matrix $\boldsymbol{B}^\perp$ has components $[\boldsymbol{B}^\perp]_{ij} = \epsilon_{ikj} \hat{b}_k$, where ϵ_{ikj} are the components of the alternating tensor. The expression $\boldsymbol{B}^\perp \cdot \boldsymbol{W}$ is sometimes written $\hat{\boldsymbol{b}} \times \boldsymbol{W}$. The contributions $\boldsymbol{W}^{(3)}$ and $\boldsymbol{W}^{(4)}$ are called the drift or gyroviscous terms. They cause no dissipation because their contraction with the strain rate tensor $\boldsymbol{W}$ vanishes. More generally, all five contributions are mutually orthogonal, in the sense that $\boldsymbol{W}^{(p)} : \boldsymbol{W}^{(q)} = 0$ for $p \neq q$. Physical interpretations of the five contributions have been given by Kaufman (1960), and further physical interpretations of the behaviour of a gyrotropic plasma have been given by Newcomb (1966).

2.2. *The viscosities*

The classical values for the viscosities of the ion fluid, in the strongly magnetised limit where $\Omega_i \tau_i \gg 1$, are

$$\eta_0 = 0.96\, n_i T_i \tau_i \qquad \text{(parallel)}, \tag{2.8a}$$

$$\eta_1 = \frac{3}{10}\frac{n_i T_i \tau_i}{(\Omega_i \tau_i)^2}, \qquad \eta_2 = 4\,\eta_1 \qquad \text{(perpendicular)}, \tag{2.8b}$$

$$\eta_3 = \frac{1}{2}\frac{n_i T_i \tau_i}{\Omega_i \tau_i}, \qquad \eta_4 = 2\,\eta_3 \qquad \text{(drift or gyro)}. \tag{2.8c}$$

Although in principle there are five independent viscosities, there are simple exact relations between η_1 and η_2, and between η_3 and η_4. The parallel viscosity η_0 is equal to the viscosity of an unmagnetised plasma, and is proportional to the ion collision time τ_i as given by

$$\tau_i = \frac{3}{4\sqrt{\pi}}\frac{\sqrt{m_i}\, T_i^{3/2}}{n_i\, e^4\, \ln \Lambda}. \tag{2.9}$$

By convention τ_i contains a factor of $\sqrt{\pi}$, while τ_e in (2.3) contains a factor of $\sqrt{2\pi}$. Viscous transport in other directions is suppressed by powers of $\Omega_i \tau_i$, where $\Omega_i = e|\boldsymbol{B}|/(m_i\, c)$ is the ion cyclotron frequency. Intuitively, the perpendicular viscosity is obtained by replacing the mean free path by the ion gyroradius, which in a strongly magnetised plasma is much smaller than the mean free path. Braginskii (1965) gave more complete expressions for the viscosities, and the thermal and electrical conductivities, that are valid for all values of $\Omega_i \tau_i$, not just in the strongly magnetised limit. Using these complete expressions, the viscous stress returns to its usual isotropic form in the weakly magnetised limit $\Omega_i \tau_i \to 0$. Revised formulae for some transport coefficients as functions of $\Omega_i \tau_i$ were given by Epperlein & Haines (1986), and a wider survey of work on transport coefficients may be found in Balescu (1988).

2.3. *Single-fluid equations*

As mentioned above, collisions between ions and electrons are much less effective at transferring energy than collisions between pairs of ions or pairs of electrons. However, on sufficiently large and slow scales the ion–electron collisions couple the two fluids sufficiently for a single fluid description to be valid. This single-fluid description, known as Braginskii MHD, resembles conventional resistive MHD apart from the use of Braginskii's expressions for the dissipative terms. It is valid for motions with frequencies below the ion cyclotron frequency Ω_i, and on length scales larger than the ion Larmor radius $\rho_i = v_{th}/\Omega_i$, where $v_{th} = (T_i/m_i)^{1/2}$ is the ion thermal velocity.

A particularly attractive theoretical model with some astrophysical relevance may be obtained by taking the incompressible limit (see e.g. Schekochihin *et al.* 2005; Craig & Litvinenko 2009). This limit is particularly relevant for the intracluster medium, for which the kinetic energy in turbulent motions is observed to be below 13 % of the thermal energy (Sanders *et al.* 2010). Moreover, the ion Alfvén velocity $v_A = B/(4\pi n_i m_i)^{1/2}$ is typically 10–30 times smaller than the ion thermal velocity (Carilli & Taylor 2002; Parrish, Stone & Lemaster 2008). There is no obstacle to an astrophysical plasma being strongly magnetised in the sense of $\Omega_i \tau_i \gg 1$, while the magnetic field is dynamically weak in the sense of $v_A \ll v_{th}$. For instance, Schekochihin *et al.* (2005) estimate that $B \gg 10^{-18}$ G is sufficient to strongly magnetise the intracluster medium, a field strength far below the observed values $B \sim 10^{-6}$ G.

Similarly, Hollweg (1986) estimates $\Omega_i \tau_i \sim 5 \times 10^5$ in an active coronal loop with $B \sim 5 \times 10^{-5}$ G.

The energy equation becomes superfluous in the incompressible limit, and is replaced by $\nabla \cdot \boldsymbol{u} = 0$. The isotropic term in (2.6*a*) may also be incorporated into the pressure, so the leading order contribution to the viscous stress becomes

$$\boldsymbol{\sigma} = 3\eta_0 \hat{\boldsymbol{b}}\hat{\boldsymbol{b}}\,\hat{\boldsymbol{b}}\hat{\boldsymbol{b}} : \nabla \boldsymbol{u}. \tag{2.10}$$

The incompressible Braginskii MHD equations may thus be written as (Schekochihin *et al.* 2005)

$$\rho \frac{\mathrm{D}\boldsymbol{u}}{\mathrm{D}t} = -\nabla p + \frac{1}{4\pi}(\nabla \times \boldsymbol{B}) \times \boldsymbol{B} + \nabla \cdot (3\eta_0 \hat{\boldsymbol{b}}\hat{\boldsymbol{b}}\hat{\boldsymbol{b}}\hat{\boldsymbol{b}} : \nabla \boldsymbol{u}), \tag{2.11a}$$

$$\frac{\partial \boldsymbol{B}}{\partial t} = \nabla \times (\boldsymbol{u} \times \boldsymbol{B}) + \lambda \nabla^2 \boldsymbol{B}, \tag{2.11b}$$

where $\lambda = c^2/(4\pi\sigma_\perp)$ is the perpendicular resistive diffusivity (Biskamp 2000). The factors of c^2 and 4π arise from using Gaussian units, rather than the $\mu_0 = 1$ units commonly used in isotropic MHD. It is a common practice in Braginskii MHD to neglect the distinction between parallel and perpendicular conductivities in (2.11*b*). These conductivities are related by $\sigma_\parallel = 1.96\,\sigma_\perp$, so there is no large disparity in conductivities comparable to the large disparity in the viscosities. Moreover, the current in the flow considered later is always perpendicular to the magnetic field, so there is no inaccuracy in using the perpendicular conductivity throughout.

The induction equation (2.11*b*) omits the Hall term that arises when passing from a two-fluid to a single-fluid description. The combination of the Hall term and the parallel and perpendicular conductivities may be written as a single tensor relation between $\boldsymbol{E}$ and $\boldsymbol{J}$, with the Hall term appearing analogous to the gyroviscous terms. However, the origins of the Hall and gyroviscous effects are completely different, and they occur on different length scales. The Hall term is due to the difference $\boldsymbol{u}_i - \boldsymbol{u}_e$ between ion and electron velocities, and its natural length scale is the ion inertial distance $d_i = c/\omega_{pi}$, where $\omega_{pi} = \left(4\pi e^2 n_i/m_i\right)^{1/2}$ is the ion plasma frequency (Biskamp 2000). By contrast, the gyro and perpendicular viscous terms are due to ions and electrons separately spirally around magnetic field lines. Their natural length scale is the ion Larmor radius $\rho_i = v_{th}/\Omega_i$. The ratio of these two length scales is

$$\frac{d_i}{\rho_i} = \frac{c}{v_{th}} \frac{\Omega_i}{\omega_{pi}} = \frac{v_A}{v_{th}}. \tag{2.12}$$

The incompressible limit described above corresponds to $v_A \ll v_{th}$, so it is consistent to neglect the Hall term while retaining the Braginskii viscous stress.

However, using the Braginskii parallel viscous stress alone, as in (2.10), leads to the viscous stress vanishing completely on the channel walls in the problem studied below. We, therefore, regularise the Braginskii MHD equations by including the perpendicular viscous stress from Braginskii's formulae (2.6*b*) and (2.6*c*) described above. This regularisation also serves to suppress the mirror and firehose instabilities that arise in Braginskii MHD when only the parallel viscous stress is included (Schekochihin *et al.* 2005).

2.4. *Relation to the Chew–Goldberger–Low theory*

The Chew, Goldberger & Low (1956) or CGL fluid equations for collisionless plasmas are another set of MHD-like equations used to describe astrophysical plasmas. This

description takes the pressure tensor to be anisotropic,

$$p_{ij} = p_\perp \delta_{ij} + (p_\parallel - p_\perp)\hat{b}_i \hat{b}_j, \tag{2.13}$$

with different pressures $p_\parallel$ and $p_\perp$ parallel and perpendicular to the magnetic field lines. The gyration of charged particles around magnetic field lines ensures isotropy of the pressure in the plane perpendicular to the magnetic fields, so a single perpendicular pressure suffices. The momentum equation is then closed by deriving evolution equations for $p_\parallel$ and $p_\perp$. The original CGL theory was closed by the 'double adiabatic' relations

$$\frac{\mathrm{D}}{\mathrm{D}t}\left(\frac{p_\perp}{\rho|\boldsymbol{B}|}\right) = 0, \quad \frac{\mathrm{D}}{\mathrm{D}t}\left(\frac{p_\parallel |\boldsymbol{B}|^2}{\rho^3}\right) = 0, \tag{2.14}$$

that hold when the heat flux may be neglected.

The Braginskii MHD momentum equation (2.11*a*) may be written in the CGL form

$$\rho \frac{\mathrm{D}\boldsymbol{u}}{\mathrm{D}t} = -\nabla p_\perp + \frac{1}{4\pi}(\nabla \times \boldsymbol{B}) \times \boldsymbol{B} + \nabla \cdot (\hat{\boldsymbol{b}}\hat{\boldsymbol{b}}(p_\perp - p_\parallel)), \tag{2.15}$$

with the closure relations for $p_\perp$ and $p_\parallel$ being given by incompressibility (which determines $p_\perp$) and

$$p_\perp - p_\parallel = 3\eta_0 \hat{\boldsymbol{b}}\hat{\boldsymbol{b}} : \nabla \boldsymbol{u}. \tag{2.16}$$

Hollweg (1986) derived this relation from the ion kinetic equation by assuming that the pressure tensor took the form (2.13), and that heat fluxes were negligible, both as in the CGL theory. However, Hollweg's (1986) derivation departed from the collisionless CGL theory by assuming that collisions were frequent enough to maintain $p_\parallel \approx p_\perp$, and that collisions acted solely to reduce pressure anisotropy while conserving internal energy. The change from a collisionless to a collisionally dominated regime is thus the main point of departure between the CGL and Braginskii theories.

3. Formulation for planar channel flow

We now adapt these general expressions for Braginskii MHD to unidirectional flow along a channel spanned by a magnetic field, the flow called Hartmann flow in conventional magnetohydrodynamics (e.g. Landau & Lifshitz 1960; Hunt & Shercliff 1971). We write the velocity and magnetic fields as

$$\boldsymbol{u} = U_0\,(0, u(x), 0)\,, \quad \boldsymbol{B} = B_0\,(1, b(x), 0), \tag{3.1}$$

where x is the coordinate across the channel, and the flow is along the channel in the y-direction. A uniform magnetic field B_0 is imposed across the channel, and the flow generates a magnetic field component $B_0 b(x)$ in the y-direction. The relevant components of the induction and momentum equations are

$$0 = -\frac{\partial p}{\partial y} + \frac{\mathrm{d}}{\mathrm{d}x}\sigma_{xy} + \frac{B_0^2}{4\pi}\frac{\mathrm{d}b}{\mathrm{d}x}, \tag{3.2a}$$

$$0 = B_0 \frac{\mathrm{d}u}{\mathrm{d}x} + \lambda\, B_0 \frac{\mathrm{d}^2 b}{\mathrm{d}x^2}. \tag{3.2b}$$

The boundary conditions are that $u = 0$ on both walls, corresponding to no-slip boundary conditions, and that $b = 0$ on both walls as well (e.g. Landau & Lifshitz 1960). The latter boundary conditions corresponds to an applied field $\boldsymbol{B} = B_0(1, 0, 0)$ outside the fluid domain, and continuity of the tangential components of the magnetic field at the walls, $[\boldsymbol{n} \times \boldsymbol{B}] = 0$. Here $\boldsymbol{n}$ is a vector normal to one of the walls, and

$[\cdot]$ denotes the jump in a quantity across the boundary. Continuity of $\boldsymbol{n} \times \boldsymbol{B}$ follows from integrating the third of Maxwell's equations (2.4) around a loop that crosses the boundary. The same boundary conditions arise from applying symmetry arguments to an infinite or periodic domain with a pressure gradient $\partial p/\partial y$ that periodically reverses direction. For example, the following boundary layer analysis applies equally well if $\partial p/\partial y$ were replaced by a body force varying sinusoidally in x. This scenario might be used to model a reversing or shearing flow across magnetic field lines in an unconfined geometry.

In this channel geometry, the only non-zero components of the strain rate tensor $\boldsymbol{W}$ are

$$W_{xy} = W_{yx} = U_0 \frac{\mathrm{d}u}{\mathrm{d}x}, \tag{3.3}$$

and the unit vector $\hat{\boldsymbol{b}}$ is given by

$$\hat{\boldsymbol{b}} = \frac{(1, b, 0)}{\sqrt{1 + b^2}}. \tag{3.4}$$

Expressions for the five contributions $\boldsymbol{W}^{(0)}$ to $\boldsymbol{W}^{(4)}$ to the viscous stress are given in the Appendix. The xy component of the total viscous stress is

$$\sigma_{xy} = \eta_0 W^{(0)}_{xy} + \eta_1 \left(W^{(1)}_{xy} + 4\, W^{(2)}_{xy} \right). \tag{3.5}$$

This may be written as

$$\sigma_{xy} = \left[\mu_\perp + (\mu_\parallel - \mu_\perp) \frac{2b^2}{(1 + b^2)^2} \right] U_0 \frac{\mathrm{d}u}{\mathrm{d}x}, \tag{3.6}$$

by defining the effective parallel and perpendicular viscosities

$$\mu_\perp = 4\,\eta_1, \quad \mu_\parallel = \tfrac{3}{2}\eta_0 - \tfrac{15}{2}\eta_1. \tag{3.7}$$

Exactly the same expression (3.6) for σ_{xy} arises from the simpler regularisation

$$\boldsymbol{\sigma} = (\mu_\parallel - \mu_\perp)\, \hat{\boldsymbol{b}}\hat{\boldsymbol{b}}\, \hat{\boldsymbol{b}}\hat{\boldsymbol{b}} : \boldsymbol{W} + \mu_\perp \boldsymbol{W}, \tag{3.8}$$

that adds a small isotropic viscous stress with viscosity $\mu_\perp$ to the leading-order anisotropic viscous stress. The perpendicular viscosity ensures that σ_{xy} remains non-zero when b vanishes. In the following, we ignore any flow perpendicular to the xy plane that is generated by the gyroviscous stress σ_{xz}.

4. Non-dimensionalisation

We rescale x by the channel width L, so the channel runs from $x = -1/2$ to $x = 1/2$ in dimensionless variables. The induction and momentum equations then become

$$B_0 U_0 \frac{\mathrm{d}u}{\mathrm{d}x} + \frac{\lambda B_0}{L} \frac{\mathrm{d}^2 b}{\mathrm{d}x^2} = 0, \tag{4.1}$$

which determines the velocity scale $U_0 = \lambda/L$, and

$$0 = F + \frac{B_0^2}{4\pi L} \frac{\mathrm{d}b}{\mathrm{d}x} + \frac{1}{L} \frac{\mathrm{d}}{\mathrm{d}x} \sigma_{xy}, \tag{4.2}$$

where $F = -\partial p/\partial y$ is the streamwise pressure gradient that drives the flow along the channel. Taking U_0 as the velocity scale is equivalent to choosing the magnetic Reynolds number $Rm = U_0 L/\lambda$ equal to unity. This justifies the use of boundary conditions on the magnetic field that were derived for the $Rm = O(1)$ regime, as in conventional Hartmann flow in isotropic MHD (e.g. Landau & Lifshitz 1960; Hunt & Shercliff 1971).

Eliminating $\mathrm{d}u/\mathrm{d}x$ using the induction equation, we obtain

$$0 = F - \frac{1}{L^3}\frac{\mathrm{d}}{\mathrm{d}x}\left[\left(\mu_\perp + (\mu_\parallel - \mu_\perp)\frac{2b^2}{(1+b^2)^2}\right)\eta\frac{\mathrm{d}^2 b}{\mathrm{d}x^2}\right] + \frac{B_0^2}{4\pi L}\frac{\mathrm{d}b}{\mathrm{d}x}. \tag{4.3}$$

We now relate the perpendicular and parallel viscosities by

$$\mu_\perp = \epsilon^2\,\mu_\parallel, \tag{4.4}$$

where $\epsilon \ll 1$ will be the basis of our asymptotic analysis. From (2.8) and (3.7), we find that $\epsilon = 0.91/(\Omega_i\tau_i)$ is inversely proportional to the dimensionless combination $\Omega_i\tau_i$ that determines the strength of the magnetisation in Braginskii's (1965) expressions for the transport coefficients.

Introducing the Hartmann number Ha, and a dimensionless measure f of the forcing strength,

$$Ha = \frac{B_0 L}{(4\pi\lambda\,\mu_\parallel)^{1/2}}, \quad f = \frac{4\pi\,FL}{B_0^2}, \tag{4.5}$$

(4.3) may be rewritten in dimensionless form as

$$0 = f - \frac{1}{Ha^2}\frac{\mathrm{d}}{\mathrm{d}x}\left[\left(\epsilon^2 + (1-\epsilon^2)\frac{2b^2}{(1+b^2)^2}\right)\frac{\mathrm{d}^2 b}{\mathrm{d}x^2}\right] + \frac{\mathrm{d}b}{\mathrm{d}x}. \tag{4.6}$$

This equation may be integrated once in x, to obtain

$$0 = fx + b - \frac{1}{Ha^2}\left(\epsilon^2 + (1-\epsilon^2)\frac{2b^2}{(1+b^2)^2}\right)\frac{\mathrm{d}^2 b}{\mathrm{d}x^2}, \tag{4.7}$$

subject to the boundary conditions $b = 0$ at $x = \pm 1/2$. We have chosen the integration constant to preserve the odd symmetry of solutions, $b(x) = -b(-x)$. The terms in (4.7) may be interpreted as a stress fx associated with the body force, a dimensionless Maxwell stress b, and a viscous stress that includes both parallel and perpendicular contributions.

For comparison, Lyutikov (2008) derived (4.7) with only parallel viscosity ($\epsilon = 0$) and then regularised it by replacing b^2 with $b^2 + \epsilon^2$ to obtain

$$0 = fx + b - \frac{2}{Ha^2}\frac{b^2+\epsilon^2}{(1+b^2+\epsilon^2)^2}\frac{\mathrm{d}^2 b}{\mathrm{d}x^2}. \tag{4.8}$$

Although this equation is different from (4.7), which we derived from Braginskii's expressions for the perpendicular viscous stress, the two equations coincide to sufficient accuracy under the scalings we introduce in § 8 to study the regions where $b = O(\epsilon)$.

Having eliminated u to obtain a single ordinary differential equation for b, the dimensionless velocity field may be reconstructed by integrating the induction equation (4.1) in x to obtain

$$u(x) = \left.\frac{\mathrm{d}b}{\mathrm{d}x}\right|_{wall} - \frac{\mathrm{d}b}{\mathrm{d}x}. \tag{4.9}$$

The gradient $\mathrm{d}b/\mathrm{d}x$ at the wall appears as an integration constant to enforce the no-slip boundary conditions $u = 0$ at the walls. The solution b is an odd function of x, so $\mathrm{d}b/\mathrm{d}x$ is the same on both walls. Moreover, $\mathrm{d}b/\mathrm{d}x$ attains its most negative value, $\mathrm{d}b/\mathrm{d}x = -f$, at the channel centre ($x = 0$). The maximum velocity is thus given by

$$u_{max} = u(0) = \left.\frac{\mathrm{d}b}{\mathrm{d}x}\right|_{wall} + f. \tag{4.10}$$

The statement $\mathrm{d}b/\mathrm{d}x = -f$ at $x = 0$ is exact for the leading-order core flow equation derived in § 6, and true up to an exponentially small error for the unapproximated equation (4.7). Further details of the behaviour near $x = 0$ are given in § 9.

5. Numerical solutions

We first describe some numerical solutions to (4.7), as shown in figures 1 and 2, before exploiting the smallness of ϵ to find asymptotic solutions. The numerical solutions shown in the figures were all computed using the two-point boundary value problem solver TWPBVPC by Cash & Mazzia (2005). This software uses an adaptive mesh placement algorithm based on the conditioning of the solution, which proved very effective at automatically placing points in the boundary layers that form near both walls when $\epsilon \ll 1$ or $Ha \gg 1$. The solutions with ϵ as small as 10^{-6} shown in figure 9 were obtained using a simple continuation technique, first computing a solution with $\epsilon = 1$ and gradually lowering ϵ while using the previous solution as an initial guess. This continuation may be required as much to allow the solver to construct a mesh with sufficient resolution near the walls as to provide an adequate initial guess for the internal Newton solver. Due to the adaptive placement of mesh points, it was straightforward to compute solutions with Hartmann numbers as large as 1000. No computation required more than 3500 points, or took more than a few seconds to run. By contrast, previous computations by Lyutikov (2008) were limited to Hartmann numbers below 10.

6. Solution in the core

We expect the streamwise magnetic field b to be $O(1)$ throughout most of the channel, as suggested by the numerical solutions. When $\epsilon \ll 1$ we thus have $b^2 \gg \epsilon^2$, so we may neglect the terms involving ϵ in (4.7) to obtain

$$0 = fx + b - \frac{1}{Ha^2} \frac{2b^2}{(1+b^2)^2} \frac{\mathrm{d}^2 b}{\mathrm{d}x^2}. \tag{6.1}$$

This equation has $b = -fx$ as an exact solution, as does (4.7) above, but otherwise appears to be analytically intractable without exploiting the Hartmann number Ha as a second parameter.

However, we may gain some insight into the structure of the solutions of (6.1) by considering small perturbations around the exact solution $b = -fx$. We write

$$b = -fx + \tilde{b}(x), \tag{6.2}$$

where $\tilde{b}(x) \ll |fx|$. The linearised form of (6.1) is

$$\tilde{b} = \frac{2f^2}{Ha^2} \frac{x^2}{(1+f^2x^2)^2} \frac{\mathrm{d}^2 \tilde{b}}{\mathrm{d}x^2}, \tag{6.3}$$

which we rewrite as

$$\frac{\mathrm{d}^2 \tilde{b}}{\mathrm{d}x^2} - \delta^2 (1+f^2x^2)^2 \frac{\tilde{b}}{x^2} = 0, \tag{6.4}$$

by introducing the parameter δ defined by

$$\delta = \frac{Ha}{\sqrt{2}f} = \frac{B_0^3}{F\sqrt{2\nu\mu_\parallel}}. \tag{6.5}$$

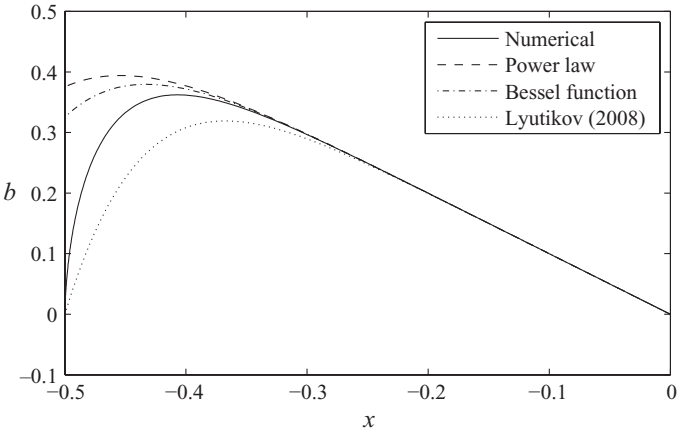

FIGURE 3. Numerical solution for $f = 1$, $Ha = 10$, $\epsilon = 10^{-3}$, and the power-law and modified Bessel function solutions to the linearised behaviour. The coefficients of these solutions were chosen by fitting to the numerical solution as $x \to 0$. Also shown is Lyutikov's (2008) approximate solution.

The linear ordinary differential equation (6.4) has a regular singular point at $x = 0$, the centre of the channel. For $|fx| \ll 1$, we may further approximate (6.4) by the homogeneous differential equation

$$\frac{\mathrm{d}^2\tilde{b}}{\mathrm{d}x^2} - \delta^2\frac{\tilde{b}}{x^2} = 0. \tag{6.6}$$

This equation has the two exact solutions $\tilde{b} = x^{r_+}$ and $\tilde{b} = x^{r_-}$. The exponents

$$r_\pm = 1/2 \pm \sqrt{\delta^2 + 1/4} \tag{6.7}$$

are the two roots of the indicial equation $r^2 - r - \delta^2 = 0$. These two roots typically differ by a non-integer value. Following the standard Frobenius theory for the solution of linear ordinary differential equations around regular singular points (e.g. Bender & Orszag 1999) both solutions of (6.6) may be developed into series solutions of (6.4),

$$\tilde{b} = x^{r_\pm}(1 + a_{2\pm}x^2 + a_{4\pm}x^4 + \cdots). \tag{6.8}$$

However, only the r_+ solution is bounded as $x \to 0$. This solution may be written as

$$\tilde{b} = x^{1/2}\mathrm{I}_{\sqrt{\delta^2+1/4}}(f\,\delta\,x), \tag{6.9}$$

in terms of the modified Bessel function I_ν with fractional order $\nu = \sqrt{\delta^2 + 1/4}$. This solution satisfies $\mathrm{d}\tilde{b}/\mathrm{d}x = 0$ at $x = 0$, because $r_+ > 1$. The boundary conditions $b = 0$ and $\mathrm{d}b/\mathrm{d}x = -f$ therefore hold at $x = 0$ for all solutions of the form (6.2).

Figure 3 compares the two linearised solutions $b = -fx + c\,\tilde{b}$ with $\tilde{b}$ given by x^{r_+} and by (6.9). The constants c for the two solutions were found by fitting to the numerical solution as $x \to 0$. The linearised solutions gives a qualitative indication of the behaviour of solutions to (6.1), but quantitative accuracy requires a numerical solution. As the magnetic field is antisymmetric in x in this channel-flow problem, it is convenient to apply $b = 0$ at $x = 0$ as one boundary condition. The above analysis shows that $x = 0$ is a regular singular point of the linearised equation, so it is legitimate to apply this boundary condition to the core equation (6.1). Lyutikov (2008) considered approximate solutions of form $b = -fx + cx^{r_+}$ and chose the

constant c so that $b = 0$ at $x = \pm 1/2$. These approximate solutions capture some of the qualitative behaviour of the true solutions, but they do not give an accurate description of the behaviour near the channel walls. In particular, they imply a width for the Hartmann boundary layers that differs from that found in § 7, and they do not capture the large gradients in b that develop near the walls.

The walls at $x = \pm 1/2$ are also singular points of (6.1), because $b = 0$ at these two points. However, they are not regular singular points because the fx term does not also vanish at these points. The behaviour of solutions near these singular points may be determined by seeking asymptotic solutions of the form $b \sim b_0(x + 1/2)^\alpha$ as $x \to -1/2$. Substituting this form into (6.1), we require

$$-\frac{1}{2} f + b_0 \left(x + \frac{1}{2}\right)^\alpha - \frac{2}{Ha^2} b_0^3 \alpha(\alpha - 1) \left(x + \frac{1}{2}\right)^{3\alpha - 2} \to 0 \quad \text{as} \quad x \to -\frac{1}{2}, \tag{6.10}$$

which determines the exponent $\alpha = 2/3$ and the coefficient b_0. The asymptotic form of the solution of (6.1) is thus

$$b \sim \tfrac{1}{2}\, 3^{2/3}\, f^{1/3}\, Ha^{2/3} \left(x + \tfrac{1}{2}\right)^{2/3} \quad \text{as} \quad x \to -\tfrac{1}{2}. \tag{6.11}$$

This solution satisfies the boundary condition $b = 0$ at $x = -1/2$, but the current $\mathrm{d}b/\mathrm{d}x$ becomes infinite at $x = -1/2$. This singularity in the current will be removed by an inner wall boundary layer, as described in § 8.

7. Hartmann layers

Equation (6.1) that describes flow in the bulk of the channel, where $|b| \gg \epsilon$, becomes analytically tractable if the Hartmann number Ha is large. The simple exact solution $b = -fx$ then holds to a good approximation over most of the domain. Deviations are confined to Hartmann layers of width $O(Ha^{-1})$ at each wall. The same scaling and qualitative behaviour is found in isotropic magnetohydrodynamics (e.g. Landau & Lifshitz 1960; Hunt & Shercliff 1971). Introducing a Hartmann boundary layer coordinate Y defined by

$$x = -\frac{1}{2} + \frac{Y}{Ha}, \tag{7.1}$$

transforms (6.1) into

$$0 = \left(-\frac{1}{2} + \frac{Y}{Ha}\right) f + b - \frac{2b^2}{(1 + b^2)^2} \frac{\mathrm{d}^2 b}{\mathrm{d}Y^2}. \tag{7.2}$$

Dropping the small $O(1/Ha)$ term leads to

$$0 = -\frac{1}{2} f + b - \frac{2b^2}{(1 + b^2)^2} \frac{\mathrm{d}^2 b}{\mathrm{d}Y^2}. \tag{7.3}$$

In physical terms, this approximation takes the total of the Maxwell and viscous stresses to be uniform, and equal to the stress on the wall.

Equation (7.3) has the form of the equation of motion for a particle moving in a time-independent potential,

$$\frac{\mathrm{d}^2 b}{\mathrm{d}Y^2} = -V'(b). \tag{7.4}$$

The potential is given by

$$V(b) = \left(b + \tfrac{1}{6} b^3 - 1/(2b)\right) f - b^2 - \log b - \tfrac{1}{4} b^4. \tag{7.5}$$

It has a single turning point, a maximum at $b = f/2$. Equation (7.4) may be integrated once using the integrating factor $\mathrm{d}b/\mathrm{d}Y$ to obtain the corresponding energy equation

$$\left(\frac{\mathrm{d}b}{\mathrm{d}Y}\right)^2 = \mathcal{E} - V(b), \tag{7.6}$$

where $\mathcal{E}$ is the integration constant.

The solution outside the Hartmann layer is given by $b = -fx + O(Ha^{-2})$, so $b \to f/2$ as $x \to -1/2$. To match the Hartmann layer solution to this outer solution, we require $B \to f/2$ as $Y \to \infty$. In terms of (7.6), this matching condition is more conveniently expressed as $\mathrm{d}b/\mathrm{d}Y \to 0$ as $b \to f/2$, which determines the constant $\mathcal{E}$ to be

$$\mathcal{E} = V\left(\tfrac{1}{2}f\right) = \tfrac{1}{192}f^4 + \tfrac{1}{4}f^2 - \log\left(\tfrac{1}{2}f\right) - 1. \tag{7.7}$$

From (7.6), we may express the solution implicitly as

$$Y = \int_0^b (\mathcal{E} - V(s))^{-1/2}\,\mathrm{d}s. \tag{7.8}$$

The lower integration limit was chosen to satisfy $b = 0$ on $Y = 0$, which corresponds to $x = -1/2$ in the original variables.

That we may take the Hartmann layer solution down to $b = 0$ requires some thought, because the ordinary differential equation (7.2) was derived by assuming $b \gg \epsilon$, and it has an irregular singular point at $Y = 0$. However, using

$$\mathcal{E} - V(s) \sim \frac{f}{2s} \quad \text{as} \quad s \to 0, \tag{7.9}$$

we may replace $\mathcal{E} - V(s)$ by just this first term in the integrand of (7.8) to obtain

$$Y \sim \frac{2^{3/2}}{3\sqrt{f}}\,b^{3/2}, \quad \text{or} \quad b \sim \tfrac{1}{2}\,3^{2/3}\,f^{1/3}\,Y^{2/3}, \quad \text{as} \quad b, Y \to 0. \tag{7.10}$$

In terms of the original variables, the asymptotic form of the Hartmann layer solution as $x \to -1/2$ is thus identical to that found previously in (6.11) by considering the behaviour of the ordinary differential equation (6.1) near its irregular singular points. The solution given by (7.8) therefore does exist as far as the wall, where $b = 0$, but as noted previously the current $\mathrm{d}b/\mathrm{d}x$ becomes infinite at the wall. This singularity will be removed by an inner wall boundary layer, as described in the next section. Figure 4 shows that numerical solutions of the original equation (4.7), when rescaled using the Hartmann layer coordinate Y, converge towards the asymptotic Hartmann layer profile given by (7.8).

The implicit solution (7.8) has a second tractable limit as $Y \to \infty$. Using $\mathcal{E} - V(s) \sim (1/2)V''(f/2)(f/2 - s)^2$ as $s \to f/2$, we may transform (7.8) into

$$\begin{aligned} Y &\sim \int_0^{f/2} (\mathcal{E} - V(s))^{-1/2} - \frac{2}{V''\left(\tfrac{1}{2}f\right)\left(\tfrac{1}{2}f - s\right)}\mathrm{d}s + \int_b^{f/2} \frac{2}{V''\left(\tfrac{1}{2}f\right)\left(\tfrac{1}{2}f - s\right)}\mathrm{d}s, \\ &\sim Y_0 - \frac{2}{V''\left(\tfrac{1}{2}f\right)}\log(1 - 2b/f), \end{aligned} \tag{7.11}$$

where $V''(f/2) = -(4 + f^2)^2/(4f^2)$. This rearranges into

$$b \sim \tfrac{1}{2}f\left[1 - \exp\left(\tfrac{1}{2}V''\left(\tfrac{1}{2}f\right)(Y_0 - Y)\right)\right] \quad \text{as} \quad Y \to \infty, \tag{7.12}$$

where the constant Y_0 must be calculated numerically from the 0 to $f/2$ integral in (7.11).

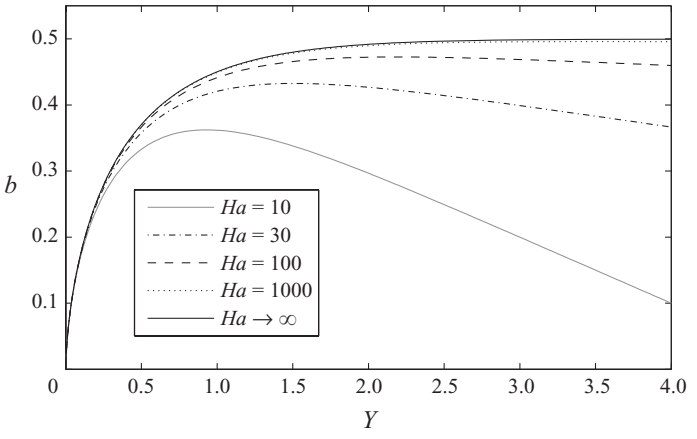

FIGURE 4. Numerical solutions for $f = 1$, $\epsilon = 10^{-3}$, and $Ha = 10$, 30, 100, 1000 rescaled into Hartmann-layer coordinates. As $Ha \to \infty$ these solutions converge towards the asymptotic Hartmann layer profile given by (7.8).

The same rescaling $x = -1/2 + Y/Ha$ leads to the standard Hartmann layers in isotropic magnetohydrodynamics. The potential function for isotropic MHD is

$$\tilde{V}(b) = bf - b^2, \tag{7.13}$$

which also has a single maximum at $b = f/2$. As before, we set $\mathcal{E} = \tilde{V}(f/2) = f^2/4$ to satisfy the matching condition $b \to f/2$ as $Y \to \infty$. The analogue of (7.8) is then

$$Y = \int_0^b \left(\frac{1}{2}f - s\right)^{-1} \mathrm{d}s = -\log(1 - 2b/f), \tag{7.14}$$

which rearranges into the familiar Hartmann layer solution of isotropic MHD (e.g. Landau & Lifshitz 1960; Hunt & Shercliff 1971)

$$b = \tfrac{1}{2} f(1 - \mathrm{e}^{-Y}). \tag{7.15}$$

Figure 5 compares this solution with the Hartmann layer solution (7.8) for Braginskii MHD, and its two asymptotic forms for $Y \to 0$ and $Y \to \infty$. All solutions are shown for $f = 1$.

8. Inner wall layers

The Hartmann layer and series solutions of the $\epsilon = 0$ equations predict infinite currents at the walls, $\mathrm{d}b/\mathrm{d}x \to \infty$ as $x \to \pm 1/2$. This is because they are based on the approximate equation (6.1) that neglects contributions from the perpendicular viscous stress. These contributions are negligible when $b \gg \epsilon$, but they become significant near the walls, where $b = O(\epsilon)$. We therefore write

$$b(x) = \frac{\epsilon}{\sqrt{2}} B(x), \tag{8.1}$$

introducing a factor of $\sqrt{2}$ for later convenience, and substitute into (4.7) to obtain

$$0 = \sqrt{2}\, fx + \epsilon\, B - \frac{\epsilon^3}{Ha^2}(1 + B^2)\frac{\mathrm{d}^2 B}{\mathrm{d}x^2}, \tag{8.2}$$

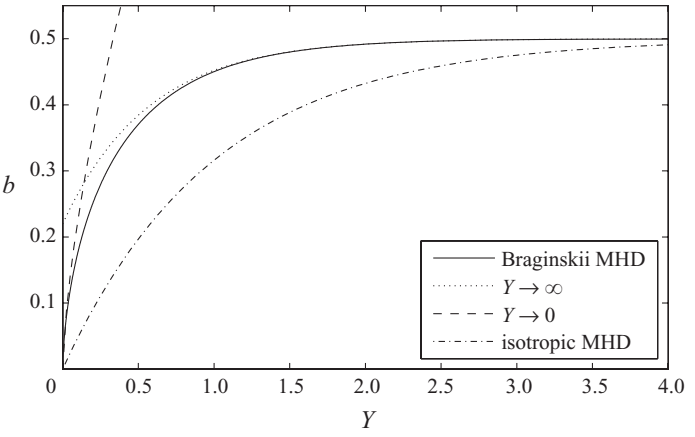

FIGURE 5. Comparison of the Hartmann layer profiles for Braginskii and isotropic MHD, both with forcing strength $f = 1$. Also shown are the two asymptotic approximations to the Braginskii MHD profile as $Y \to 0$ and $Y \to \infty$. The Braginskii profile has an infinite gradient at $Y = 0$, which must be resolved by an inner wall layer as calculated in § 8.

after neglecting smaller terms in the viscous stress. This rescaling of b has brought the parallel and perpendicular contributions to the viscous stress into balance with each other. The same leading-order equation (8.2) results from substituting (8.1) into Lyutikov's (2008) *ad hoc* regularised equation (4.8), and neglecting small terms.

To bring the viscous stress into balance with the forcing term, we introduce the inner wall layer coordinate X defined by

$$x = -\frac{1}{2} + \frac{\epsilon^{3/2}}{2^{1/4} f^{1/2} Ha} X, \tag{8.3}$$

to obtain

$$0 = -\frac{1}{2}\left(1 - \frac{2^{3/4}\epsilon^{3/2}}{f^{1/2} Ha} X\right) + \frac{\epsilon}{2^{1/2} f^{1/2}} B - (1 + B^2)\frac{\mathrm{d}^2 B}{\mathrm{d}X^2}. \tag{8.4}$$

Dropping further terms of $O(\epsilon)$ and smaller from (8.4) leads to a universal equation for the magnetic field within the inner wall layer,

$$0 = -\frac{1}{2} - (1 + B^2)\frac{\mathrm{d}^2 B}{\mathrm{d}X^2}. \tag{8.5}$$

This universal form was achieved by including the Hartmann number Ha and the dimensionless forcing strength f in the definition of the inner wall layer coordinate X. In physical terms, we assume that the total viscous stress within the wall layer is spatially uniform, and equal to the stress applied on the wall. The Maxwell stress is now negligibly small, while the earlier Hartmann layer was defined by a balance between the Maxwell stress and the parallel viscous stress. Unlike the previous section, the analysis in this section does not require a large Hartmann number. The inner wall layers, whose scale is defined by X, fit between the wall and any Hartmann layer that is present if $Ha \gg 1$.

Equation (8.5) must be solved subject to the boundary conditions

$$B = 0 \text{ at } X = 0, \quad \text{and} \quad \frac{\mathrm{d}B}{\mathrm{d}X} \to 0 \quad \text{as} \quad B \to \infty. \tag{8.6}$$

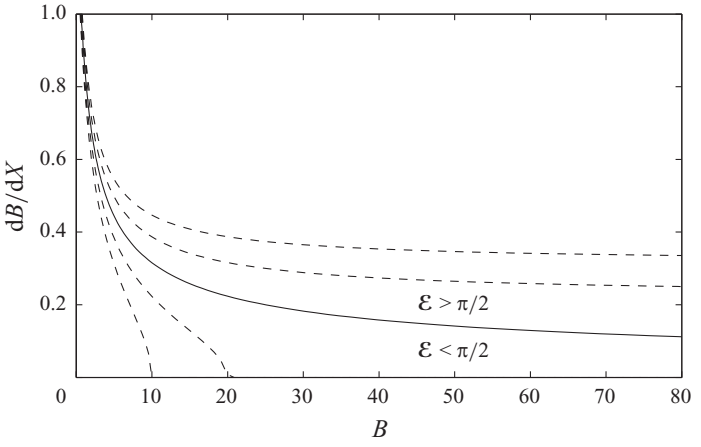

FIGURE 6. Phase plane for the ODE in (8.8). The trajectory with $\mathcal{E} = \pi/2$ (shown as solid line) is the only trajectory for which $\mathrm{d}B/\mathrm{d}X \to 0$ as $B \to \infty$. The other trajectories, shown as dotted lines, have $\mathcal{E} = \pi/2 \pm 0.05$ and $\mathcal{E} = \pi/2 \pm 0.1$.

The first boundary condition is inherited from $b = 0$ at $x = -1/2$ in the original dimensionless variables, while the second is the matching condition that results from the relation

$$\frac{\mathrm{d}B}{\mathrm{d}X} = \frac{2^{1/4}\epsilon^{1/2}}{f^{1/2}\,Ha}\,\frac{\mathrm{d}b}{\mathrm{d}x} \tag{8.7}$$

for rescaling derivatives into the wall-layer variables. The core solution has $\mathrm{d}b/\mathrm{d}x = O(1)$, which implies $\mathrm{d}B/\mathrm{d}X = O(\epsilon^{1/2})$ becomes small as $X \to \infty$. Perhaps surprisingly, we do not need any further details of the solution in the core to find the solution in the wall layer, only the fact that $\mathrm{d}B/\mathrm{d}X$ becomes asymptotically small in the core. This differs from the behaviour of a Hartmann layer solution, whose magnitude is determined by matching to the flow in the core.

Equation (8.5) again has the form of an equation of motion for a particle in a potential. Multiplying by $(1 + B^2)^{-1}\mathrm{d}B/\mathrm{d}X$ and integrating with respect to X, we obtain

$$\left(\frac{\mathrm{d}B}{\mathrm{d}X}\right)^2 + \tan^{-1} B(X) = \mathcal{E}. \tag{8.8}$$

The integration constant $\mathcal{E}$ is analogous to the particle's energy. As $B = 0$ at $X = 0$, we may also interpret $\mathcal{E}^{1/2}$ as the current $\mathrm{d}B/\mathrm{d}X$ at the wall. The phase plane for solutions of (8.8) is shown in figure 6. The second boundary condition in (8.6) determines $\mathcal{E} = \pi/2$. Solutions of (8.8) with $\mathcal{E} < \pi/2$ terminate at finite values of B, while solutions with $\mathcal{E} > \pi/2$ have $\mathrm{d}B/\mathrm{d}X = O(1)$ as $B \to \infty$. In other words, there is only one value of $\mathcal{E}$ that allows the solution to match to an outer region. This solution has just enough energy for the particle to escape to infinity with zero residual velocity. It may be written implicitly as

$$X = \int_0^B (\cot^{-1} s)^{-1/2}\,\mathrm{d}s, \tag{8.9}$$

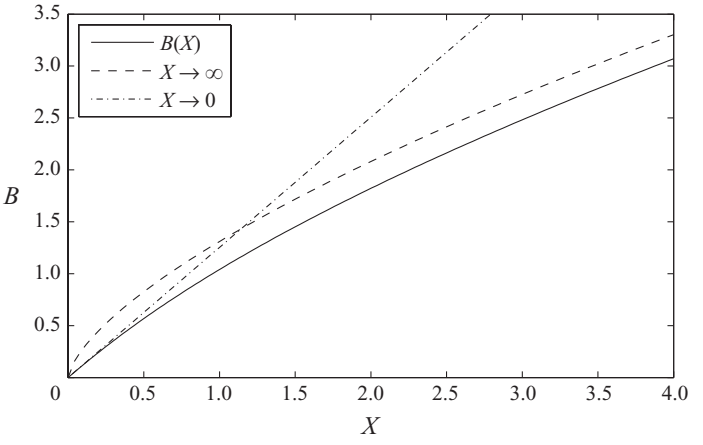

FIGURE 7. The universal inner wall layer function $B(X)$ given implicitly by (8.9), and its asymptotic forms $B \sim (3X/2)^{2/3}$ as $X \to \infty$ and $B \sim (\pi/2)^{1/2} X$ as $X \to 0$.

by using the trigonometric identity $\cot^{-1} s = \pi/2 - \tan^{-1} s$. Using the asymptotic expansion $\cot^{-1} s \sim 1/s + O(s^{-3})$ for large s, we recover

$$B \sim \left(\tfrac{3}{2}X\right)^{2/3} \quad \text{as} \quad X \to \infty. \tag{8.10}$$

Undoing the changes of variables that define B and X, we obtain

$$b \sim \tfrac{1}{2}\, 3^{2/3}\, f^{1/3}\, Ha^{2/3} \left(x + \tfrac{1}{2}\right)^{2/3} \quad \text{as} \quad X \to \infty. \tag{8.11}$$

The outer limit of the wall layer solution thus coincides with the inner limit (6.11) of the Hartmann layer and series solutions. This confirms the correctness of the matching conditions imposed on both solutions. Replacing the integrand in (8.9) by its limiting value, $\cot^{-1} s \to \pi/2$ as $s \to 0$, gives the behaviour of the solution in the other limit,

$$B \sim \left(\tfrac{1}{2}\pi\right)^{1/2} X \quad \text{as} \quad X \to 0. \tag{8.12}$$

The full solution (8.9) and its asymptotic approximations (8.10) and (8.12) are plotted in figure 7. Figure 8 shows that the numerical solutions, when rescaled into the inner wall layer variables B and X, converge as $\epsilon \to 0$ to the limiting form given by (8.9).

Transforming back into the original variables, the current b_x at the wall is

$$b_x\left(\pm\tfrac{1}{2}\right) = 2^{-3/4}\pi^{1/2} f^{1/2}\, Ha\, \epsilon^{-1/2}, \tag{8.13}$$

and, from (4.10), the maximum velocity is

$$u_{max} = 2^{-3/4}\pi^{1/2} f^{1/2}\, Ha\, \epsilon^{-1/2} + f. \tag{8.14}$$

Neither results depends upon a detailed computation of the solution in the core. Figure 9 shows a comparison of the theoretical result for u_{max} with numerical solutions for $f = 1$ and three different Hartmann numbers, $Ha = 1$, 10, 100, over the range $10^{-6} \leqslant \epsilon \leqslant 1$. The agreement is very satisfactory for $\epsilon \leqslant 0.1$. Figure 8 shows that for $\epsilon = 0.1$ the gradient of the numerical solution at the wall is in good agreement with the asymptotic theory, even though the solution elsewhere departs substantially from the asymptotic form.

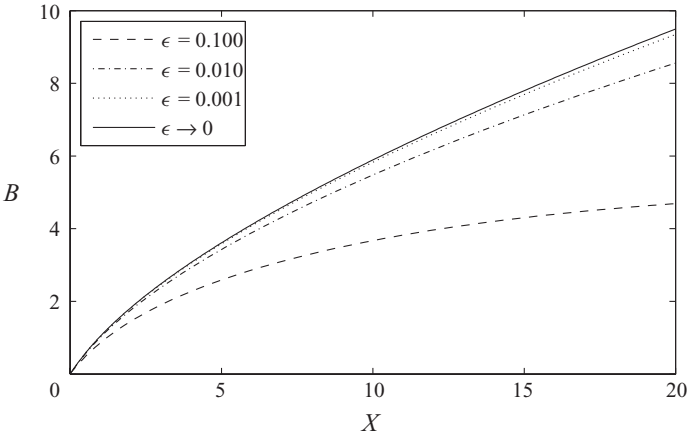

FIGURE 8. Numerical solutions for $f = 1$, $Ha = 10$, and $\epsilon = 0.1$, 0.01, 0.001 rescaled into inner wall layer coordinates. These solutions converge towards the universal inner wall layer function (8.9) as $\epsilon \to 0$.

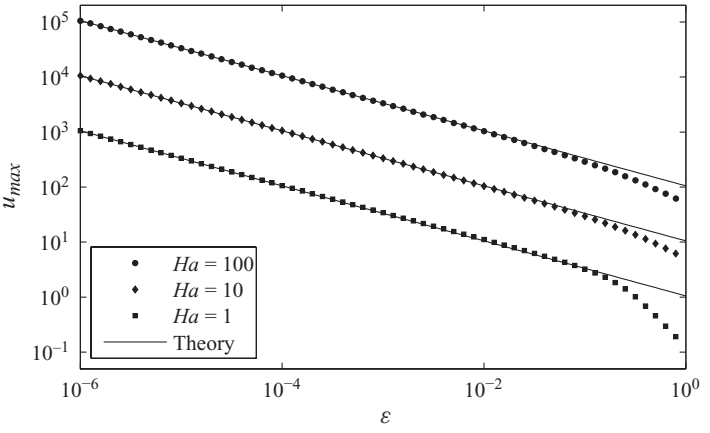

FIGURE 9. Maximum speed for $f = 1$ and $Ha = 1$, 10, 100 from numerical solutions compared with the theoretical formula (8.14).

9. Inner central region

Having investigated the behaviour near the walls, where $b = O(\epsilon)$, for completeness we now investigate the behaviour near $x = 0$, where also $b = O(\epsilon)$. The ordinary differential equation describing the behaviour in the core, where $b \gg \epsilon$, has a regular singular point at $x = 0$. This singular point disappears when we restore the terms involving ϵ. Substituting $b = -fx + \tilde{b}(x)$ into (4.7), linearising for small $\tilde{b}$, and further approximating for small x yields,

$$\frac{\mathrm{d}^2\tilde{b}}{\mathrm{d}x^2} = \frac{\delta^2}{\tilde{\epsilon}^2 + x^2}\tilde{b}, \tag{9.1}$$

where $\tilde{\epsilon} = \sqrt{2}\epsilon/f$. When $x \gg \tilde{\epsilon}$ this reduces to the previous homogeneous equation (6.6) that has a regular singular point at $x = 0$. However, the ordinary differential equation (9.1) is regular at $x = 0$, due to the $\tilde{\epsilon}^2$ term in the denominator. For $|x| \ll \tilde{\epsilon}$, its solutions behave like $\exp(\pm\delta x/\tilde{\epsilon})$.

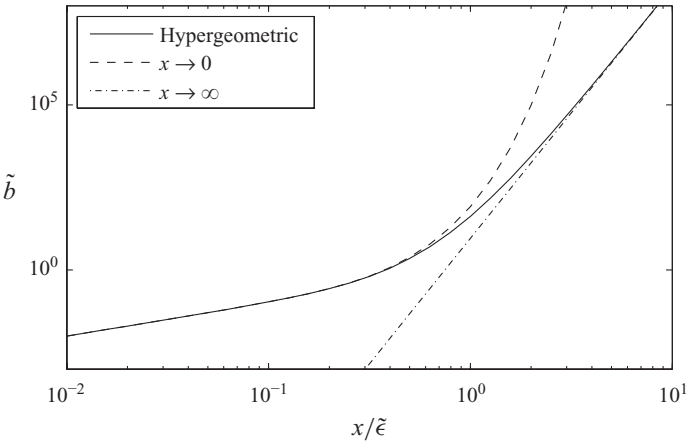

FIGURE 10. The hypergeometric function solution that resolves the regular singular point at $x = 0$ in the $\epsilon = 0$ equations. The behaviour for $x \gg \epsilon$ coincides with the $\tilde{b} \sim x^{r_+}$ solution 'found in § 6, but the hypergeometric solution has a non-zero gradient at $x = 0$. The natural normalization leads to a unit gradient at $x = 0$. The solution shown has $f = 1$ and $Ha = 10$, so $\delta = 5\sqrt{2}$ and $r_+ \approx 7.6$.

These two different behaviours are connected by the solution of (9.1) that satisfies $\tilde{b} = 0$ at $x = 0$. This solution may be written in terms of the ${}_2F_1$ hypergeometric function (Abramowitz & Stegun 1965) as

$$\tilde{b} = Z(1 + Z^2)\,{}_2F_1\left(1 + \tfrac{1}{2}r_+, 1 + \tfrac{1}{2}r_-; \tfrac{3}{2}; -Z^2\right), \tag{9.2}$$

where $Z = x/\tilde{\epsilon}$, and $r_\pm = 1/2 \pm \sqrt{\delta^2 + 1/4}$ are the two roots of the indicial equation from (6.7). Applying formula (15.3.7) from Abramowitz & Stegun (1965),

$${}_2F_1(a, b; c; -z) \sim \frac{\Gamma(c)\Gamma(b-a)}{\Gamma(b)\Gamma(c-a)} z^{-b} \quad \text{as} \quad z \to \infty \text{ when } a > b, \tag{9.3}$$

to (9.2) we obtain

$$\tilde{b} \sim \frac{\sqrt{\pi}\,\Gamma\left(\frac{1}{2}r_+ - \frac{1}{2}r_-\right)}{2\Gamma(1 + \frac{1}{2}r_+)\Gamma\left(\frac{1}{2} - \frac{1}{2}r_-\right)} Z^{r_+} \quad \text{as} \quad Z \to \infty, \tag{9.4}$$

which is consistent with the analysis of § 6. The other limit is

$$\tilde{b} \sim \sinh(\delta Z)/\delta \quad \text{as} \quad Z \to 0, \tag{9.5}$$

so the solution for $\tilde{b}$ given by (9.2) has a non-zero derivative at $x = 0$. The regular singular point in the $\epsilon = 0$ limiting equation (6.1) is thus alleviated by an $O(\epsilon)$-wide layer around $x = 0$. The linearised solution $\tilde{b}$ in this layer has non-zero derivative at $x = 0$, but becomes indistinguishable from the x^{r_+} solution of (6.1) when $x \gg \epsilon$. The plotted solution (9.4) is shown normalised to have unit derivative at $x = 0$. However, the solution of the full ordinary differential equation has $\tilde{b}$ very small in this inner $x \sim \tilde{\epsilon}$ region. From the approximate power-law solution, we estimate $\tilde{b} \sim |2x|^{r_+}$ so that $\tilde{b} = O(1)$ when $x = \pm 1/2$. This implies $\tilde{b} \sim \epsilon^{r_+}$ when $x \sim \epsilon$ at the outer edge of this central region. From the two limiting forms of the hypergeometric solution, we then estimate $\tilde{b}_x \sim \epsilon^{r_+} e^{-\delta}$ at $x = 0$.

10. Conclusion

Braginskii magnetohydrodynamics offers a single-fluid description of large-scale motions in strongly magnetised plasmas. In these plasmas, the gyrofrequency of ions spirally around magnetic field lines is much larger than the ion collision frequency. Equivalently, the ion Larmor radius is much smaller than the mean free path. Momentum transport perpendicular to the magnetic field is then strongly suppressed, so the viscous stress is directed predominantly parallel to the magnetic field lines, as given by (1.1).

Equation (1.1) is commonly taken to be the complete viscous stress in Braginskii MHD, but some further contribution is necessary if we are to satisfy the boundary conditions for Hartmann flow. Integrating the streamwise momentum equation across the channel from $x = 0$ to $x = L$ gives

$$0 = -L\frac{\partial p}{\partial y} + \left[B_0^2 b + \sigma_{xy}\right]_0^L. \tag{10.1}$$

The magnetic boundary conditions are $b = 0$ at the walls $x = 0$ and $x = L$. The Maxwell stress $B_0^2 b$ and the parallel viscous stress $\sigma_{xy}^{(0)}$ therefore both also vanish at the walls. This leaves nothing to balance the streamwise pressure gradient.

We have resolved this difficulty by extending Braginskii MHD to include the perpendicular viscous stress given by the $\boldsymbol{W}^{(1)}$ and $\boldsymbol{W}^{(2)}$ tensors. This contribution does not vanish at the walls, and so transmits the streamwise pressure gradient to the walls as required for a steady-state global momentum balance. For a unidirectional flow and a planar magnetic field, the perpendicular contribution from the $\boldsymbol{W}^{(1)}$ and $\boldsymbol{W}^{(2)}$ tensors is precisely the same as the contribution from a phenomenological isotropic viscous stress. However, we have ignored the extra gyroviscous stress from the $\boldsymbol{W}^{(3)}$ and $\boldsymbol{W}^{(4)}$ tensors that would tend to drive a flow perpendicular to the plane of the channel.

The suppression of momentum transport perpendicular to magnetic field lines implies that the perpendicular viscosity $\mu_\perp$ is much smaller than the parallel viscosity $\mu_\parallel$. Our dimensionless equations contain a small parameter $\epsilon = (\mu_\perp/\mu_\parallel)^{1/2}$, the square root of the viscosity ratio. In terms of more common plasma parameters, $\epsilon = \sqrt{5/6}\,(\Omega_i \tau_i)^{-1}$, where Ω_i is the ion gyrofrequency, and τ_i is the ion collision time. The numerical prefactor comes from the prefactors in Braginskii's (1965) expressions for the viscosities, as given in (2.8). A strongly magnetised plasma is thus characterised by $\epsilon \ll 1$.

Setting $\epsilon = 0$ leads to an equation that holds in the core of the channel, and describes the limiting behaviour of the magnetic field (only) as $\epsilon \to 0$. This equation has a regular singular point at the channel centre, and *irregular* singular points at the channel walls. Further analytical progress is possible when the Hartmann number is large. Deviations from the simple exact solution $b = -fx$ are then confined to Hartmann boundary layers of width $O(Ha^{-1})$ next to the walls. These Hartmann layers are governed by a balance between the Maxwell stress and the parallel viscous stress. The sum of these two stresses is spatially uniform, and equal to the total stress applied to the wall by the streamwise pressure gradient. Boundary conditions for the Hartmann layer solution were found by matching to the core, and by imposing $b = 0$ at the walls. This solution confirms the result of the series solution around the irregular singular points in predicting an infinite current at the walls. The asymptotic form of the current is $b_x \sim |x - x_{wall}|^{-1/3}$ as $x \to x_{wall}$.

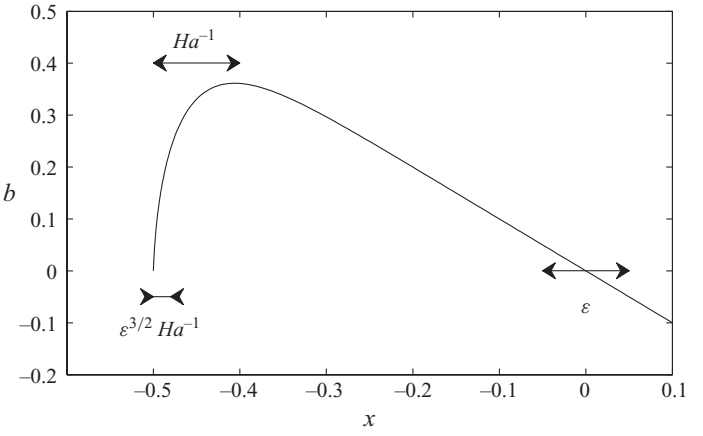

FIGURE 11. Regime diagram summarising the different asymptotic regions: the Hartmann layers of width $O(Ha^{-1})$, the inner wall layers of width $O(\epsilon^{3/2}Ha^{-1})$, and the central region of width $O(\epsilon)$. Elsewhere the solution is given by $b \approx -fx$.

The singularities at the walls are removed by the perpendicular viscous stress, which becomes significant close to the walls where $b = O(\epsilon)$. The resulting rescaling reveals a second set of boundary layers that are $O(\epsilon^{3/2})$ wide and adjacent to each wall. These inner wall layers fit inside the Hartmann layers that are present when $Ha \gg 1$. The Maxwell stress is negligibly small in the inner wall layers, while the viscous stress is spatially uniform and equal to the stress at the wall. The magnetic field in the inner wall layers is given by the universal form (8.9) in suitably rescaled variables. The current at the walls is thus made finite, but the peak current scales as $\epsilon^{-1/2}$ as given by (8.13). The different asymptotic regions are summarised in figure 11.

The current and the velocity are related by the integrated induction equation (4.9). The large current at the wall is joined by a large shear, so the maximum velocity also scales as $\epsilon^{-1/2}$. The velocity reaches this large value at the edge of the inner wall boundary layers, but then varies relatively little across the core of the flow. In other words, our asymptotic analysis of Braginskii MHD, as regularised by perpendicular viscosity, shows that the peak velocity grows indefinitely as ϵ, the ratio of perpendicular to parallel viscosities, tends to zero. The large shear at the walls may be predicted by considering a global stress balance, as given by (10.1). The streamwise pressure gradient must be balanced by the stress on the channel walls. The Maxwell stress vanishes because the magnetic field is locally perpendicular to the channel walls, and so does the parallel contribution to the viscous stress. Therefore, the pressure gradient must be balanced entirely by the perpendicular viscous stress on the walls. Since the perpendicular viscosity is very small, the shear at the walls must be very large to give an order-unity perpendicular viscous stress. The solution of the Hartmann flow problem thus has no limiting form as the viscosity ratio tends to zero.

The main conclusion of this study is that large shears and currents develop in boundary layers whose scale is linked to the small ratio of perpendicular to parallel viscosities wherever there is shear perpendicular to magnetic field lines. Such shear may be expected to arise generically in the turbulent astrophysical flows currently modelled using Braginskii MHD, and the solution then depends critically on the value of the viscosity ratio. This study is open to extension in a number of directions.

Although the inner wall layers described in §8 are widely applicable, requiring only that the combination $\epsilon^3/(fHa^2)$ be small, we have implicitly assumed that $f = O(1)$ in calculating the Hartmann layers in §7. When $f \gg 1$ the correct scale for the streamwise magnetic field becomes fB_0, rather than B_0, because the strong shear stretches the initial spanwise field to create a field with a large streamwise component. The scale of the Maxwell stress then become fB_0^2, and the width of the Hartmann layers shrinks from Ha^{-1} to $(fHa)^{-1}$. We have also neglected the out-of-plane flow parallel to the z-axis that is driven by the gyroviscous stresses. This flow would create further gyroviscous stresses and modify the original planar flow. Finally, planar incompressible MHD commonly arises in the context of reduced MHD, in which incompressibility is maintained by a strong, almost uniform magnetic field perpendicular to the plane. An additional out-of-plane component to the magnetic field would change the expressions for the viscous stress given in the Appendix, and would also lead to a non-zero parallel current. However, the key ingredient of this study, the vanishing of the parallel viscous stress in regions of shear, exists in all of these other scenarios.

The author thanks A. Schekochihin for introducing him to Braginskii magnetohydrodynamics, and M. Rosin for useful conversations. The author's research is supported by an Advanced Research Fellowship, grant EP/E054625/1, from the UK Engineering and Physical Sciences Research Council.

Appendix A. Expressions for the $\boldsymbol{W}$ tensors

The tensors $\boldsymbol{W}^{(0)}$ to $\boldsymbol{W}^{(4)}$ for the planar channel flow under consideration are

$$\boldsymbol{W}^{(0)} = U_0 \frac{\mathrm{d}u}{\mathrm{d}x} \frac{3b}{(1+b^2)^2} \begin{pmatrix} 1 & b & 0 \\ b & b^2 & 0 \\ 0 & 0 & 0 \end{pmatrix}, \tag{A 1a}$$

$$\boldsymbol{W}^{(1)} = U_0 \frac{\mathrm{d}u}{\mathrm{d}x} \frac{b}{(1+b^2)^2} \begin{pmatrix} -b^2 & b & 0 \\ b & -1 & 0 \\ 0 & 0 & 1+b^2 \end{pmatrix}, \tag{A 1b}$$

$$\boldsymbol{W}^{(2)} = U_0 \frac{\mathrm{d}u}{\mathrm{d}x} \frac{1-b^2}{(1+b^2)^2} \begin{pmatrix} -2b & 1-b^2 & 0 \\ 1-b^2 & 2b & 0 \\ 0 & 0 & 0 \end{pmatrix}, \tag{A 1c}$$

$$\boldsymbol{W}^{(3)} = U_0 \frac{\mathrm{d}u}{\mathrm{d}x} \frac{b}{(1+b^2)^{3/2}} \begin{pmatrix} 0 & 0 & b \\ 0 & 0 & -1 \\ b & -1 & 0 \end{pmatrix}, \tag{A 1d}$$

$$\boldsymbol{W}^{(4)} = U_0 \frac{\mathrm{d}u}{\mathrm{d}x} \frac{1-b^2}{(1+b^2)^{3/2}} \begin{pmatrix} 0 & 0 & 1 \\ 0 & 0 & b \\ 1 & b & 0 \end{pmatrix}. \tag{A 1e}$$

REFERENCES

Abramowitz, M. & Stegun, I. A. 1965 *Handbook of Mathematical Functions*. Dover.

Balbus, S. A. 2004 Viscous shear instability in weakly magnetized, dilute plasmas. *Astrophys. J.* **616**, 857–864.

Balescu, R. 1988 *Transport Processes in Plasmas: Classical Transport Theory*. North-Holland.

Bender, C. M. & Orszag, S. A. 1999 *Advanced Mathematical Methods for Scientists and Engineers*. Springer.

Biskamp, D. 2000 *Magnetic Reconnection in Plasmas*. Cambridge University Press.

Braginskii, S. I. 1965 Transport processes in a plasma. *Rev. Plasma Phys.* **1**, 205–311.

Carilli, C. L. & Taylor, G. B. 2002 Cluster magnetic fields. *Annu. Rev. Astron. Astrophys.* **40**, 319–348.

Cash, J. R. & Mazzia, F. 2005 A new mesh selection algorithm, based on conditioning, for two-point boundary value codes. *J. Comput. Appl. Math.* **184**, 362–381.

Cercignani, C. 1988 *The Boltzmann Equation and its Applications*. Springer.

Chapman, S. & Cowling, T. G. 1970 *The Mathematical Theory of Non-Uniform Gases*, 3rd edn. Cambridge University Press.

Chew, G. F., Goldberger, M. L. & Low, F. E. 1956 The Boltzmann equation and the one-fluid hydromagnetic equations in the absence of particle collisions. *Proc. R. Soc. Lond. Ser.* A **236**, 112–118.

Craig, I. J. D. & Litvinenko, Y. E. 2009 Anisotropic viscous dissipation in three-dimensional magnetic merging solutions. *Astron. Astrophys.* **501**, 755–760.

Dong, R. & Stone, J. M. 2009 Buoyant bubbles in intracluster gas: effects of magnetic fields and anisotropic viscosity. *Astrophys. J.* **704**, 1309–1320.

Dorf, L., Sun, X., Intrator, T., Hendryx, J., Wurden, G., Furno, I. & Lapenta, G. 2007 Experimental verification of Braginskii's viscosity in MHD plasma jet of reconnection scaling experiment. *Bull. APS* **52**, PM4.00007.

Epperlein, E. M. & Haines, M. G. 1986 Plasma transport coefficients in a magnetic field by direct numerical solution of the Fokker–Planck equation. *Phys. Fluids* **29**, 1029–1041.

Furno, I., Intrator, T., Torbert, E., Carey, C., Cash, M. D., Campbell, J. K., Fienup, W. J., Werley, C. A., Wurden, G. A. & Fiksel, G. 2003 Reconnection scaling experiment: a new device for three-dimensional magnetic reconnection studies. *Rev. Sci. Instrum.* **74**, 2324–2331.

Grad, H. 1949 On the kinetic theory of rarefied gases. *Comm. Pure Appl. Math.* **2**, 331–407.

Grad, H. 1958 Principles of the kinetic theory of gases. In *Thermodynamik der Gase* (ed. S. Flügge), Handbuch der Physik, vol. 12, pp. 205–294. Springer.

Hogan, J. T. 1984 Collisional transport of momentum in axisymmetric configurations. *Phys. Fluids* **27**, 2308–2312.

Hollweg, J. V. 1986 Viscosity and the Chew–Goldberger–Low equations in the solar corona. *Astrophys. J.* **306**, 730–739.

Hunt, J. C. R. & Shercliff, J. A. 1971 Magnetohydrodynamics at high Hartmann number. *Annu. Rev. Fluid Mech.* **3**, 37–62.

Islam, T. & Balbus, S. 2005 Dynamics of the magnetoviscous instability. *Astrophys. J.* **633**, 328–333.

Kaufman, A. N. 1960 Plasma viscosity in a magnetic field. *Phys. Fluids* **3**, 610–616.

Landau, L. D. & Lifshitz, E. M. 1960 *Electrodynamics of Continuous Media*, Pergamon.

Lifshitz, E. M. & Pitaevskii, L. P. 1981 *Physical Kinetics*. Pergamon.

Lyutikov, M. 2008 Hartmann flow with Braginsky viscosity: a test problem for plasma in the intracluster medium. *Astrophys. J. Lett.* **673**, L115–L117.

Newcomb, W. A. 1966 Dynamics of a gyroviscous plasma. In *Dynamics of Fluids and Plasmas* (ed. S. I. Pai), pp. 405–429. Academic.

Parrish, I. J., Stone, J. M. & Lemaster, N. 2008 The magnetothermal instability in the intracluster medium. *Astrophys. J.* **688**, 905–917.

Sanders, J. S., Fabian, A. C., Smith, R. K. & Peterson, J. R. 2010 A direct limit on the turbulent velocity of the intracluster medium in the core of Abell 1835 from XMM–Newton. *Mon. Not. R. Astron. Soc.* **402**, L11–L15.

Schekochihin, A., Cowley, S., Kulsrud, R., Hammett, G. & Sharma, P. 2005 Magnetised plasma turbulence in clusters of galaxies. In *The Magnetized Plasma in Galaxy Evolution* (ed. K. T. Chyzy, K. Otmianowska-Mazur, M. Soida & R.-J. Dettmar), pp. 86–92. Jagiellonian University, Krakow, Poland.

Sharma, P., Quataert, E., Hammett, G. W., & Stone, J. M. 2007 Electron heating in hot accretion flows. *Astrophys. J.* **667**, 714–723.

Spitzer, L. 1962 *Physics of Fully Ionized Gases*. Wiley.